Chiral Recognition with High-Energy Photo- and Compton Electrons: A Theoretical Showcase Study of Methyloxirane and Trifluoromethyloxirane Molecules

Daniel M. Haubenreißer,[1] Nikolay M. Novikovskiy,[1] Max Kircher,[2] Markus S. Schöffler,[2] Reinhard Dörner,[2] Till Jahnke,[3,4] and Philipp V. Demekhin[1,*]

[1]*Institut für Physik und CINSaT, Universität Kassel, Heinrich-Plett-Strasse 40, 34132 Kassel, Germany*
[2]*Institut für Kernphysik, Goethe-Universität Frankfurt, Max-von-Laue-Strasse 1, 60438 Frankfurt am Main, Germany*
[3]*Max-Planck-Institut für Kernphysik, Saupfercheckweg 1, 69117 Heidelberg, Germany*
[4]*European XFEL, Holzkoppel 4, 22869 Schenefeld, Germany*

(Received 9 July 2025; revised 20 September 2025; accepted 3 November 2025; published 20 November 2025)

We report a comparative theoretical study of molecular-frame angular emission distributions of high-energy electrons released from the O 1*s* inner shell of methyloxirane and trifluoromethyloxirane molecules via photoionization and, alternatively, ionization by a Compton scattering of high-energy photons. We demonstrate that the high-energy photo- and Compton electrons can be employed to determine the absolute configuration of these chiral molecules via diffraction imaging. This is particularly important in cases where the single-molecule handedness cannot be recognized from ionic fragmentation patterns. Thereby, we establish high-energy photoionization and ionization by Compton scattering as additional complementary tools for chiral recognition in the gas phase.

DOI: 10.1103/4fnf-wkfd

One of the most powerful and well-established techniques for chiral recognition in the gas phase relies on the fundamental effect of photoelectron circular dichroism (PECD) [1–5]. The effect is based on the fact that low-energy photoelectrons escape a molecular ion slowly and have thus sufficient time to respond to the chiral asymmetry of the molecule's potential. This results in the enantio- and helicity-sensitive forward-backward asymmetry in the photoemission [6–8] (with respect to the light propagation direction), and this asymmetry survives averaging over random molecular orientations. An alternative tool to access an absolute configuration (or handedness) of a chiral molecule (on a single-molecule level) is Coulomb explosion imaging (CEI) [9]. This method provides (comparably direct) information on the spatial arrangement of constituents of a molecule. The approach relies on a rapid charge up of the molecule: After being multiply charged, the molecule undergoes an ultrafast disintegration, where ionic fragments are driven apart by Coulomb repulsion. If the momentum vectors of more than three molecular fragments are measured in a CEI experiment, the handedness of a chiral molecule can be determined [10–12].

Although CEI has a broad potential for deducing molecular handedness, there are many technical challenges that constrain the application of this technique in real life. Particularly challenging are the ultrafast generation of highly charged states of the molecule and the coincident detection of many ionic fragments. The latter can be achieved nowadays for up to 5–7 ions given typical ion detection efficiencies [13]. Furthermore, uncertainties in the m/q assignment or breakdown of the axial recoil approximation [14] increase the technical challenges. Therefore, in the past, PECD and CEI measurement concepts were successfully combined to improve chiral recognition in the gas phase. On the one hand, confining the spatial orientation of molecules (fully or partly) results in considerably stronger forward-backward asymmetries of the emitted photoelectrons [15–19], increasing thereby the sensitivity to enantiomeric excess drastically. On the other hand, inspecting the angular emission distributions of low-energy photoelectrons in a molecular frame of reference can be used for chiral recognition. This is especially useful, if the molecule's handedness cannot be recognized from the information gathered by CEI alone [18–20]. Such molecular-frame photoelectron angular distributions (MFPADs) [21–24] provide the most complete information on the molecular structure and dynamics.

While there are no doubts about the enantiosensitivity of low-energy electrons discussed above [1–5], high-energy electrons are commonly assumed to be enantioinsensitive. This is because a high-energy photoelectron wave packet leaves the molecular ion rather quickly and has no time to adopt to its chiral asymmetry.

*Contact author: demekhin@physik.uni-kassel.de

Published by the American Physical Society under the terms of the Creative Commons Attribution 4.0 International license. Further distribution of this work must maintain attribution to the author(s) and the published article's title, journal citation, and DOI.

Nevertheless, high-kinetic-energy electrons allow one to access structural and dynamical information via photoelectron diffraction imaging [25–28]. In particular, their MFPADs exhibit forward-scattering lobes pointing (away from the emitter site) in the directions of heavy neighbors [28,29], whose nucleus acts as lenses for the emerging electron wave. Moreover, a superposition of the directly emitted and on-the-neighbor-scattered photoelectron waves creates rich double-slit interference patterns that can directly be related with a distance between the emitter and the scatterer [28,29]. Most importantly, these properties of the high-energy MFPADs persist in the polarization-averaged molecular-frame photoelectron angular distributions (PA-MFPADs) [30,31]. This is very beneficial from an experimental point of view, since a larger fraction of the measured dataset can be used for the analysis of the molecular handedness.

In the present Letter, we demonstrate theoretically that molecular-frame diffraction patterns of high-energy electrons can be used to recognize whether a chiral molecule was right- or left-handed. In particular, we show that this is possible even in cases when employing only a partial ionic breakup, i.e., in a case where CEI alone cannot provide this information. For this purpose, we use the showcases of methyloxirane (C_3H_6O, MOx) and trifluoromethyloxirane ($C_3H_3F_3O$, TFMOx) molecules and study ionization of their O 1s inner shell by two different light-driven mechanisms. Specifically, we consider photoionization and ionization by Compton scattering of high-energy photons [32,33] and demonstrate that both mechanisms can be used for chiral sensing in the gas phase. In the latter case, the chiral recognition relies on the recently uncovered scattering of direct Compton electrons on the parent [34,35] and neighboring [36] nuclei. The resulting diffraction patterns in the molecular-frame electron momentum distribution survive an averaging over the photon momentum transfer and enable electron diffraction imaging of molecules through the Compton ionization mechanism [36].

In order to recognize the handedness of a chiral molecule via CEI [10–12], one needs a molecule to break up into (i) at least four fragments, (ii) four of which preferably contain atoms heavier than hydrogen, and (iii) at least three of them are charged. The requirements (i) and (ii) ensure that the three momenta measured in (iii) can be noncoplanar. For small chiral molecules (such as the considered here MOx, which contains only four atoms heavier than hydrogen), such a breakup scenario is rather improbable. The proposed O 1s ionization of MOx results often in prominent incomplete breakup channels that consist of ionic and neutral molecular fragments, as, for example [18,20], $C_3H_6O + \hbar\omega \rightarrow C_2H^+_{2,3} + CH^+_2 + OH^0_{2,1} + e^-_{ph} + e^-_{Aug}$. Here, it is important that the (typically) undetectable neutral fragment $OH^0_{2,1}$ contains a heavy oxygen atom. As a consequence, two momentum vectors of the ionic fragments $C_2H^+_{2,3}$ and CH^+_2, measured via CEI, are not collinear and thus build a plane, which is, however, identical for both molecular enantiomers.

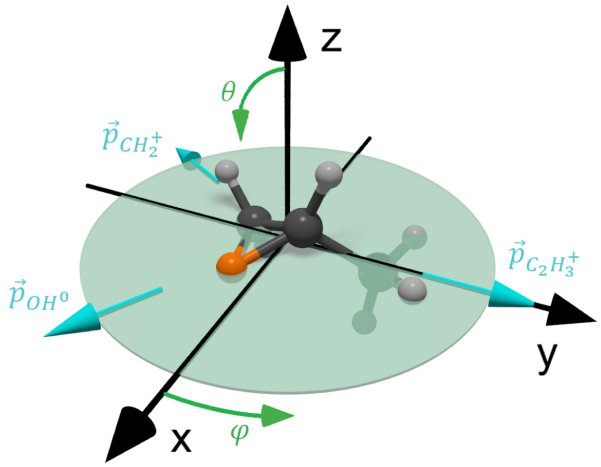


FIG. 1. Molecular-frame coordinate system of S-methyloxirane, defined in Refs. [18,20] with the help of the measured fragment momenta (turquoise arrows) as follows: $\vec{y} = \vec{p}_{C_2H^+_{2,3}}$, $\vec{z} = \vec{p}_{C_2H^+_{2,3}} \times \vec{p}_{CH^+_2}$, and $\vec{x} = \vec{y} \times \vec{z}$. The momenta allow for an unambiguous definition of the x-y plane (highlighted in green color), but not for the determination of the molecular handedness.

Accordingly, this breakup channel cannot be used for determination of the absolute configuration, but it may be employed for defining a molecular frame of reference. The molecular-frame coordinate system of the S-methyloxirane, constructed in Refs. [18,20] for this breakup, is shown in Fig. 1 (see its caption for the definition).

For the photoionization process, an averaging over the light polarization is equivalent to an integration over all directions from which the ionizing light of a given polarization impinges onto the molecule. As a consequence, in an experiment, much more ionization events contribute to a PA-MFPAD for a fixed-in-space molecule (as compared to an MFPAD). Thereby, targeting a PA-MFPAD for extraction of the molecular configuration yields larger experimental statistics (or requires less acquisition time). PA-MFPADs are also identical for linear and circularly polarized light, which makes them accessible at most synchrotron or x-ray free-electron laser beam lines. From the theoretical side, such an averaging can be performed analytically, and an explicit expression for the PA-MFPAD can be found in our previous works [19,20]. Below, we derive the corresponding observable for Compton scattering, i.e., the molecular-frame Compton electron angular distribution (MFCEAD), which we average over the photon momentum transfer for the same reasons. To the lowest order of perturbation theory, the $\hat{A}^2$ operator governs ionization via the Compton scattering of high-energy photons [37,38]. Here, one of the vector potential operators annihilates the incident photon with the momentum $\vec{k}_\gamma$, and another creates the scattered photon with the momentum $\vec{k}_{\gamma'}$. This event corresponds to the photon momentum transfer $\vec{Q} = \vec{k}_\gamma - \vec{k}_{\gamma'}$ and an emission

of an electron with momentum $\vec{p}$ from a bound state Ψ_i into a continuum state $\Psi_{\vec{p}}^-$.

The total transition amplitude for Compton ionization reads [35,36] (atomic units are used throughout)

$$A_{\vec{Q}}(\vec{p}) = \langle \Psi_{\vec{p}}^- | e^{i\vec{Q}\cdot\vec{r}} | \Psi_i \rangle. \quad (1)$$

Making use of a partial-wave expansion for the electron wave function $\Psi_{\vec{p}}^-$ in the continuum with a kinetic energy of $\varepsilon = p^2/2$ [39,40]

$$\Psi_{\vec{p}}^-(\vec{r}) = \sum_{\ell m} (i)^\ell R_{\varepsilon\ell m}(r) Y_{\ell m}(\hat{r}) Y_{\ell m}^*(\hat{p}), \quad (2)$$

we obtain

$$A_{\vec{Q}}(\vec{p}) = \sum_{\ell m} (-i)^\ell \langle \Psi_{\varepsilon\ell m} | e^{i\vec{Q}\cdot\vec{r}} | \Psi_i \rangle Y_{\ell m}(\hat{p}). \quad (3)$$

Here, $\hat{p}$ stands for the electron emission angles $\{\theta, \varphi\}$, and, for transparency, we incorporated normalization coefficients and scattering phase shifts in the radial parts of the partial electron waves $\Psi_{\varepsilon\ell m}(\vec{r}) = R_{\varepsilon\ell m}(r) Y_{\ell m}(\hat{r})$ with the angular momentum quantum numbers ℓ and m. The amplitude (3) can be further simplified by expanding the plane-wave operator $e^{i\vec{Q}\cdot\vec{r}}$ in terms of spherical waves [41]

$$A_{\vec{Q}}(\vec{p}) = \sum_{\ell m k q} (-i)^\ell i^k A_{\varepsilon\ell m k q}(Q) Y_{kq}^*(\hat{Q}) Y_{\ell m}(\hat{p}), \quad (4)$$

with the following definition of the matrix element:

$$A_{\varepsilon\ell m k q}(Q) = 4\pi \langle \Psi_{\varepsilon\ell m} | j_k(Qr) Y_{kq}(\hat{r}) | \Psi_i \rangle. \quad (5)$$

Here, $j_k(Qr)$ are the spherical Bessel functions.

Taking the modulus square of the amplitude (4) and reducing the product of two spherical functions to one [41], we arrive at the following expansion for the MFCEAD for a given photon momentum transfer vector $\vec{Q}$:

$$\frac{d\sigma}{d\Omega_p}(\vec{Q}, \hat{p}) = \sum_{LM} B_{LM}(\vec{Q}) Y_{LM}^*(\hat{p}). \quad (6)$$

The analytic expression for the expansion coefficients B_{LM} in Eq. (6) reads

$$\begin{aligned} B_{LM}(\vec{Q}) = & \sum_{\ell m k q} \sum_{\ell' m' k' q'} i^{\ell+\ell'+k+k'} (-1)^{\ell+m'+k'} \\ & \times \sqrt{\frac{(2\ell+1)(2\ell'+1)(2L+1)}{4\pi}} \\ & \times \begin{pmatrix} \ell & \ell' & L \\ 0 & 0 & 0 \end{pmatrix} \begin{pmatrix} \ell & \ell' & L \\ m & -m' & M \end{pmatrix} \\ & \times A_{\varepsilon\ell m k q}(Q) A_{\varepsilon\ell' m' k' q'}^*(Q) \\ & \times Y_{kq}^*(\hat{Q}) Y_{k'q'}(\hat{Q}). \end{aligned} \quad (7)$$

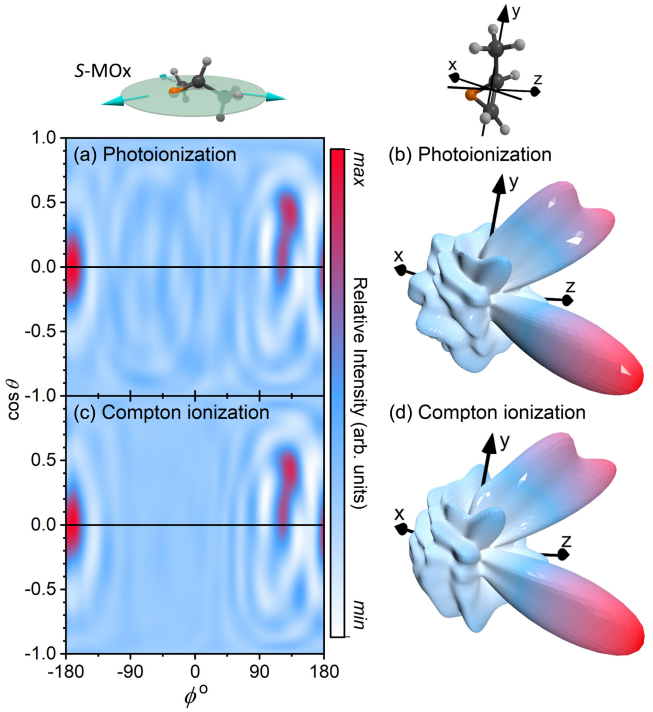


FIG. 2. PA-MFPAD (a) and QA-MFCEAD (c) for the O 1s ionization of S-methyloxirane, computed for the electron kinetic energy of 200 eV. (b),(d) Three-dimensional representations of, respectively, (a) and (c), where the distance from the origin indicates the emission probability. The molecular orientation for (b) and (d) is visualized in the inset.

In order to access the $\vec{Q}$-averaged molecular-frame Compton electron angular distributions (QA-MFCEAD), the expansion coefficients $B_{LM}(\vec{Q})$ (7) need to be integrated over the magnitude Q and orientation $\hat{Q}$ of the photon momentum transfer vector. The former integration has to be performed numerically, while the latter can be done analytically, using the orthogonality property of spherical functions: $\int Y_{kq}^*(\hat{Q}) Y_{k'q'}(\hat{Q}) d\Omega_Q = \delta_{kk'}\delta_{qq'}$.

The present calculations were carried out by the single-center method and code [42–44], similar to our previous works on the MOx [15,18,20] and TFMOx [16,17,19] molecules. The numerical calculations were performed in the frozen-core Hartree-Fock approximation including partial electron continuum waves $\Psi_{\varepsilon\ell m}$ with angular momenta up to $\ell, |m| \leq 29$, while orbitals of the bound electrons were represented by the single-center expansions with $\ell_b, |m_b| \leq 99$. In the case of photoionization, one tunes the energy of the ionizing photon to release photoelectrons with particular kinetic energy. On the contrary, Compton scattering of x-ray photons with a well-defined high energy releases electrons with a continuous momentum spectrum from zero to approximately $2\vec{k}_\gamma$ (which corresponds to the photon's backscattering). In the present Letter, we considered Compton scattering of 20 keV

photons with $|\vec{k}_\gamma| = 5.37$ a.u. The matrix elements (5) were computed numerically for values of Q ranging from 0.5 to 10.5 a.u. in steps of 0.5 a.u.

Below, we discuss our computational results on the MOx molecule, performed for electron kinetic energies of $\varepsilon = 200$ eV (Fig. 2) and 400 eV (Fig. 3). Two different representations are used for the PA-MFPAD in Figs. 2(a) and 2(b) and QA-MFCEAD in Figs. 2(c) and 2(d), both computed for the O 1s ionization of the S enantiomer of MOx. In Figs. 2(a) and 2(c), the two-dimensional emission probability, as a function of the electron emission angles θ and φ in the molecular frame of reference, is shown as a color-coded map (see Fig. 1 for definitions of the molecular coordinate system and the angles). The green plane depicted in the inset above Fig. 2(a), which is defined by the molecular fragment momenta (turquoise arrows), corresponds to the black horizontal line at $\cos\theta = 0$ in Figs. 2(a) and 2(c). These distributions are shown again in Figs. 2(b) and 2(d) in a three-dimensional representation (see caption of the figure for details). The orientation of the molecule in the given coordinate frame is visualized in the inset above Fig. 2(b).

First of all, we notice that the QA-MFCEAD in Figs. 2(c) and 2(d) are very similar to the PA-MFPAD in Figs. 2(a) and 2(b). In particular, they exhibit very similar and distinct main lobes pointing toward the heavy neighboring atoms. In addition, both show double-slit-like interference patterns (with a slightly reduced contrast for the Compton ionization). This means that the electronic potential of the molecular ion, which governed the multiple scattering of emitted electrons, shapes both distributions, and the ionization mechanism itself does not play a decisive role. By looking at the molecular orientation, visualized in the inset above Figs. 2(b) and 2(d), one can recognize that the strongest single lobe points from the emitter (oxygen atom) toward the carbon atom in the oxirane ring. The lower one from the two overlapping lobes points toward the carbon atom in the chiral center, and the upper lobe points toward the carbon atom in the methyl group. In the two-dimensional color maps of Figs. 2(a) and 2(c), the strongest single lobe is seen as a red spot around $\cos\theta \approx 0$ and $\varphi \approx \pm 180°$, which corresponds to the x-y plane and negative direction of the x axis (see also Fig. 1 for the mutual orientation of the oxygen atom and the carbon atom from the oxirane ring). From the two overlapping lobes, the first one, which points toward the carbon atom in the chiral center, appears as a red spot around $\cos\theta \approx +0.4$ and $\varphi \approx +130°$. It is more prominent than the second one because of the smaller distance between the emitter and the scatterer. The second slightly weaker lobe, pointing toward the carbon atom in the methyl group, appears as a red stripe at around $\cos\theta \approx 0$ and $\varphi \approx +120°$. Because of the overlap of the two lobes, the maximum of the weaker one is shifted toward the stronger one. The double-slit interference patterns appear in the two-dimensional representation of Figs. 2(a) and 2(c) as the overlapping blue color (maxima) and white color (minima) oval fringes. As one can already imagine, the lobe pointing toward the chiral center with $\cos\theta \approx +0.4$ can be used for the recognition of the molecular handedness.

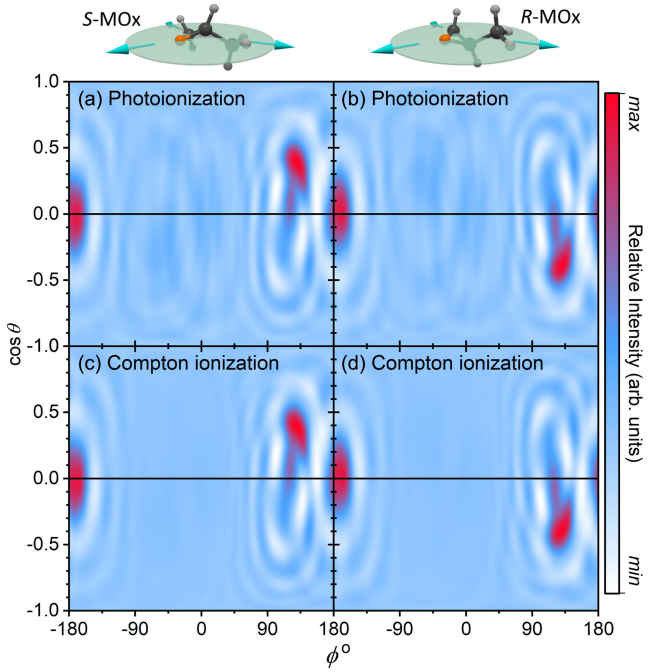


FIG. 3. PA-MFPADs (a),(b) and QA-MFCEAD (c),(d) for the O 1s ionization of S- (a),(c) and R- (b),(d) enantiomers of methyloxirane (see insets atop), computed for an electron kinetic energy of 400 eV. The electron angular distributions of the two enantiomers are mirror images of each other with respect to the horizontal line at $\cos\theta = 0$ (i.e., the green plane in the insets).

This fact is demonstrated explicitly in Fig. 3, which depicts the PA-MFPAD [Figs. 3(a) and 3(b)] and QA-MFCEAD [Figs. 3(c) and 3(d)], computed for an electron kinetic energy of $\varepsilon = 400$ eV and two different enantiomers of the molecule. Figures 3(a) and 3(c) represent the S-MOx, while Figs. 3(b) and 3(d) the R-MOx (see respective insets on top of the figure, which are vertical mirror images of each other, i.e., mirrored at the horizontal green plane). As one can see again, the ionization mechanism does not play a significant role, since the PA-MFPAD and QA-MFCEAD computed for a particular enantiomer are very similar to each other. Because of the larger kinetic energy (electron momentum), there are now considerably more interference fringes seen in the blue-white-colored ovals, as compared to lower electron energy used in Fig. 2. Most importantly, the distributions, computed for the opposite enantiomers, are indeed mirror images of each other with respect to the black horizontal line located at $\cos\theta = 0$ (i.e., $z \leftrightarrow -z$). As a consequence, the red spot representing the main lobe pointing toward the chiral center emerges above or below this line (plane) in the angular distributions belonging to the two enantiomers.

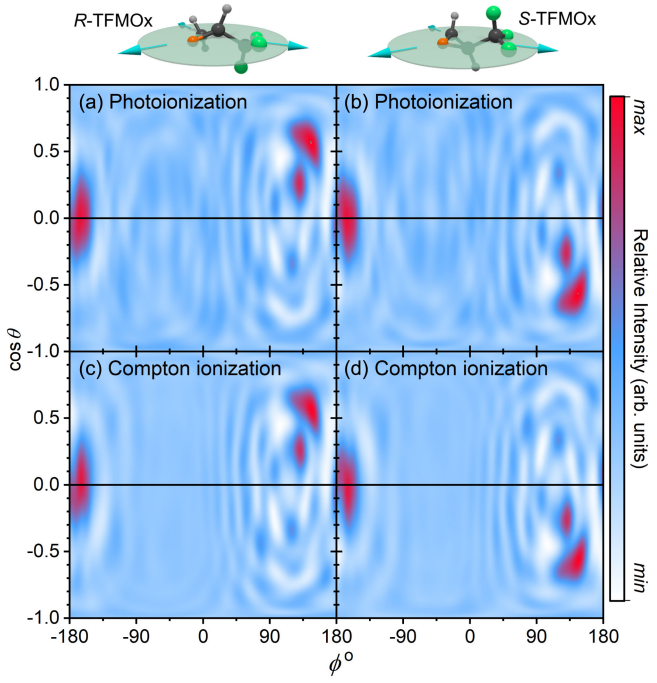


FIG. 4. The same as in Fig. 3, but for the O 1s ionization of R- (a),(c) and S- (b),(d) enantiomers of trifluoromethyloxirane (see insets atop) and the electron kinetic energy of 200 eV. The main lobe pointing toward the chiral center appears above (for R-TFMOx) or below (for S-TFMOx) the horizontal line at $\cos\theta = 0$ (i.e., the green plane in the insets) and, thus, unambiguously identifies the molecular handedness.

Figure 4 supports that the results discussed in this Letter are of general nature. In particular, it demonstrates a possibility to assign enantiomers of the TFMOx molecule with the 200 eV photo- and Compton electrons by considering its incomplete breakup channel $C_3H_3F_3O + \hbar\omega \rightarrow CF_3^+ + C_2H_2^+ + OH^0 + e_{ph}^- + e_{Aug}^-$ [19], which cannot be used alone to recognize molecular handedness. Along the line of generality, a demonstration of the experimental feasibility of structure recognition using high-energy electrons has been, so far, performed with respect to employing photoelectrons only. Photoelectron diffraction imaging of small molecules in the gas phase allowed, for example, to determine bond lengths in a static [29], as well as in a time-resolved scenario [28]. The concept of employing an incomplete breakup has been demonstrated in Refs. [18–20]. Experimentally, much more challenging are corresponding measurements using Compton ionization, as the absolute cross section for Compton scattering is substantially lower. Thus, a measurement requires high flux of hard x-ray photons provided, e.g., by high-repetition-rate x-ray free-electron lasers or latest generation synchrotrons. Still, high-dimensional measurements investigating molecules have been performed in the past, including the measurement of MFCEADs [36]. The extension to imaging of larger (and chiral) molecules is a logical next step and corresponding measurements are underway.

In conclusion, we demonstrated theoretically that high-energy electrons released by photoionization or via ionization by Compton scattering of high-energy photons can be used for recognition of chiral molecules in the gas phase. The discrimination between two enantiomers can be achieved via electron diffraction imaging of a chiral molecule, even if its absolute configuration cannot be deduced by Coulomb explosion imaging. Here, we made use of the forward-scattering lobes in the molecular-frame electron emission distributions, which point toward the heavy neighbors and survive averaging over the light polarization for the photoionization and over the photon momentum transfer for the Compton ionization. The present finding extends the concept of light-driven chiral recognition in the gas phase toward intermediate and hard x-ray domains.

Acknowledgments—The authors acknowledge Robert Berger for valuable discussions. This work was funded by the Deutsche Forschungsgemeinschaft (DFG)–Project No. 328961117–SFB 1319 ELCH (Extreme light for sensing and driving molecular chirality).

Data availability—The data that support the findings of this Letter are not publicly available. The data are available from the authors upon reasonable request.

[1] I. Powis, Adv. Chem. Phys. **138**, 267 (2008).
[2] L. Nahon, G. A. Garcia, and I. Powis, J. Electron Spectrosc. Relat. Phenom. **204**, 322 (2015).
[3] S. Turchini, J. Phys. Condens. Matter **29**, 503001 (2017).
[4] R. Hadidi, D. K. Bozanic, G. A. Garcia, and L. Nahon, Adv. Phys. X **3**, 1477530 (2018).
[5] C. Sparling and D. Townsend, Phys. Chem. Chem. Phys. **27**, 2888 (2025).
[6] B. Ritchie, Phys. Rev. A **12**, 567 (1975).
[7] B. Ritchie, Phys. Rev. A **14**, 359 (1976).
[8] B. Ritchie, Phys. Rev. A **13**, 1411 (1976).
[9] Z. Vager, R. Naaman, and E. P. Kanter, Science **244**, 426 (1989).
[10] M. Pitzer, M. Kunitski, A. S. Johnson, T. Jahnke, H. Sann, F. Sturm, L. Ph. H. Schmidt, H. Schmidt-Böcking, R. Dörner, J. Stohner, J. Kiedrowski, M. Reggelin, S.Marquardt, A. Schießer, R. Berger, and M. S. Schöffler, Science **341**, 1096 (2013).
[11] K. Fehre, S. Eckart, M. Kunitski, M. Pitzer, S. Zeller, C. Janke, D. Trabert, J. Rist, M. Weller, A. Hartung, L. Ph. H. Schmidt, T. Jahnke, R. Berger, R. Dörner, and M. S. Schöffler, Sci. Adv. **5**, eaau7923 (2019).
[12] M. Pitzer, G. Kastirke, P. Burzynski, M. Weller, D. Metz, J. Neff, M. Waitz, F. Trinter, L. Ph. H. Schmidt, J. B. Williams, T. Jahnke, H. Schmidt-Böcking, R. Berger, R. Dörner, and M. Schöffler, J. Phys. B **49**, 234001 (2016).
[13] R. Boll *et al.*, Nat. Phys. **18**, 423 (2020).
[14] R. N. Zare, Mol. Photochem. **4**, 1 (1972), https://web.stanford.edu/group/Zarelab/publinks/zarepub60.pdf.

[15] M. Tia *et al.*, J. Phys. Chem. Lett. **8**, 2780 (2017).
[16] G. Nalin *et al.*, Phys. Chem. Chem. Phys. **23**, 17248 (2021).
[17] K. Fehre, F. Trinter, N. M. Novikovskiy, S. Grundmann, D. Tsitsonis, S. Eckart, L. Bauer, M. Hilzinger, T. Jahnke, R. Dörner, Ph. V. Demekhin, and M. S. Schöffler, Phys. Chem. Chem. Phys. **24**, 13597 (2022).
[18] K. Fehre *et al.*, Phys. Rev. Lett. **127**, 103201 (2021).
[19] G. Nalin *et al.*, Phys. Rev. Res. **5**, 013021 (2023).
[20] K. Fehre *et al.*, Phys. Chem. Chem. Phys. **24**, 26458 (2022).
[21] A. Landers, Th. Weber, I. Ali, A. Cassimi, M. Hattass, O. Jagutzki, A. Nauert, T. Osipov, A. Staudte, M. H. Prior, H. Schmidt-Böcking, C. L. Cocke, and R. Dörner, Phys. Rev. Lett. **87**, 013002 (2001).
[22] T. Jahnke *et al.*, Phys. Rev. Lett. **88**, 073002 (2002).
[23] J. B. Williams, C. S. Trevisan, M. S. Schöffler, T. Jahnke, I. Bocharova, H. Kim, B. Ulrich, R. Wallauer, F. Sturm, T. N. Rescigno, A. Belkacem, R. Dörner, Th. Weber, C. W. McCurdy, and A. L. Landers, Phys. Rev. Lett. **108**, 233002 (2012).
[24] H. Fukuzawa, R. R. Lucchese, X.-J. Liu, K. Sakai, H. Iwayama, K. Nagaya, K. Kreidi, M. S. Schöffler, J. R. Harries, Y. Tamenori, Y. Morishita, I. H. Suzuki, N. Saito, and K. Ueda, J. Chem. Phys. **150**, 174306 (2019).
[25] F. Krasniqi, B. Najjari, L. Strüder, D. Rolles, A. Voitkiv, and J. Ullrich, Phys. Rev. A **81**, 033411 (2010).
[26] M. Kazama, T. Fujikawa, N. Kishimoto, T. Mizuno, J. I. Adachi, and A. Yagishita, Phys. Rev. A **87**, 063417 (2013).
[27] R. Boll *et al.*, Faraday Discuss. **171**, 57 (2014).
[28] G. Kastirke *et al.*, Phys. Rev. X **10**, 021052 (2020).
[29] I. Vela-Peréz *et al.*, Phys. Chem. Chem. Phys. **25**, 13784 (2023).
[30] F. Ota, K. Yamazaki, D. Sébilleau, K. Ueda, and K. Hatada, J. Phys. B **54**, 024003 (2021).
[31] F. Ota, K. Hatada, D. Sébilleau, K. Ueda, and K. Yamazaki, J. Phys. B **54**, 084001 (2021).
[32] M. J. Cooper, Rep. Prog. Phys. **48**, 415 (1985).
[33] M. J. Cooper, P. E. Mijnarends, N. Shiotani, N. Sakai, and A. Bansil, *X-Ray Compton Scattering*, Oxford Science Publications, Vol. 5 (Oxford University Press, Oxford, New York, 2004).
[34] M. Kircher, F. Trinter, S. Grundmann, I. Vela-Perez, S. Brennecke, N. Eicke, J. Rist, S. Eckart, S. Houamer, O. Chuluunbaatar, Y. V. Popov, I. P. Volobuev, K. Bagschik, M. N. Piancastelli, M. Lein, T. Jahnke, M. S. Schöffler, and R. Dörner, Nat. Phys. **16**, 756 (2020).
[35] N. Melzer *et al.*, Phys. Rev. Lett. **133**, 183002 (2024).
[36] D. M. Haubenreißer *et al.*, Phys. Rev. Lett. **135**, 033203 (2025).
[37] P. M. Bergstrom, Jr. and R. H. Pratt, Radiat. Phys. Chem. **50**, 3 (1997).
[38] K. Pisk, Z. Kaliman, and N. Erceg, J. Phys. B **49**, 235004 (2016).
[39] A. F. Starace, *Theory of Atomic Photoionization.* Handbook of Physics, Vol. 31 (Springer, Berlin, 1982).
[40] N. A. Cherepkov, J. Phys. B **14**, 2165 (1981).
[41] D. A. Varshalovich, A. N. Moskalev, and V. K. Khersonsky, *Quantum Theory of Angular Momentum* (World Scientific, Singapore, 1988).
[42] Ph. V. Demekhin, A. Ehresmann, and V. L. Sukhorukov, J. Chem. Phys. **134**, 024113 (2011).
[43] S. A. Galitskiy, A. N. Artemyev, K. Jänkälä, B. M. Lagutin, and Ph. V. Demekhin, J. Chem. Phys. **142**, 034306 (2015).
[44] N. M. Novikovskiy, A. N. Artemyev, D. V. Rezvan, B. M. Lagutin, and Ph. V. Demekhin, J. Phys. B **55**, 175001 (2022).